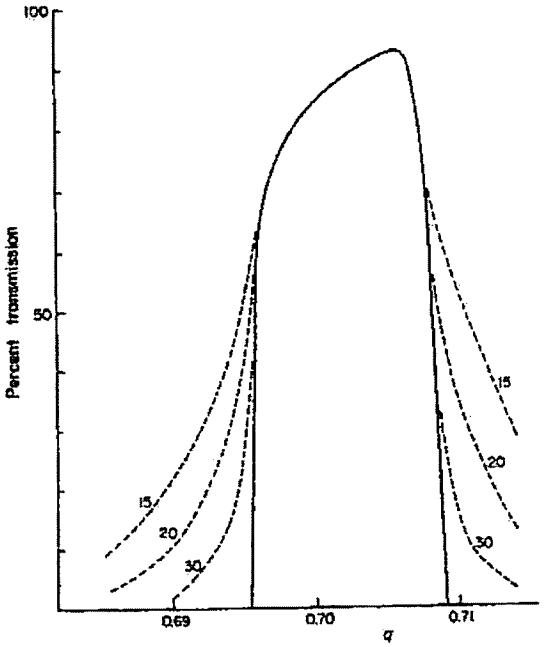

Fig. 5.3. A peak shape by a detailed computer simulation for an ion beam entering parallel to the instrument axis when there is a fringing field through which the ions take two cycles to pass. The broken lines indicate the shapes for fields limited in length to the stated number of rf cycles.

3 cycles long are beneficial. When the fields are longer than 3 cycles, there is a large reduction in instrument aperture (unless a delayed d.c. ramp is used). The curve labelled 4.5* shows a calculation for a ramp which increases quadratically as the ion approaches the mass filter entrance. Similar calculations for the xz plane are illustrated in Fig. 5.2. Averaged over all phases, even long entrance ramps are beneficial in the x direction.

The detailed computer simulations of mass filter performance by matrix methods (see Chapter II, p. 31) have been repeated including the presence of a two-cycle field [7]. Again, a beam entering parallel to the instrument axis was considered. There was an increase in transmission throughout most of the rf cycle and a decrease of the dependence on the zero and $\pi/2$ phases (cf. Fig. 2.20). Figure 5.3 shows some computed peak shapes. A comparison with the peak shapes for "perfect" fields (Fig. 2.21) indicates an increase of usable aperture area by a factor of three or four.

The introduction into the calculations of a realistic length for the mass filter is associated with "tailing" on the side of the peaks, particularly on the low mass side. The decrease of importance of the zero and $\pi/2$ phases in the presence of the fringing fields results in less peak tailing and more symmetrical peaks.

All the illustrations of fringing field effects given above consider the simplified case of ion beams parallel to the instrument axis with no angular divergence. Phase-space dynamics (see Chapter IV) provides a more complete

analysis and permits the evaluation of ion source/lens combinations. The acceptance of the mass filter without fringing fields was illustrated in Figs. 2.14 and 2.15. The acceptance ellipses are characterized by the parameters A, B, Γ and ϵ where

$$\Gamma u^2 + 2Auu' + Bu'^2 = \epsilon \tag{5.1}$$

Considering the usual two-dimensional linear approximation with separation of ion motion in the yz and xz planes, the effect of a fringing field can be represented in matrix form by

$$\begin{bmatrix} u \\ u' \end{bmatrix}_e = \begin{bmatrix} C & S \\ C' & S' \end{bmatrix} \begin{bmatrix} u \\ u' \end{bmatrix}_a \tag{5.2}$$

where u_e and u'_e are the position and velocity at the point where the full mass filter field begins and u_a and u'_a those at the entrance aperture in front of the quadrupole where the fringing field begins. It is then readily shown [9] that the overall acceptance of the mass filter with its fringing field is characterized by A_a, B_a, Γ_a and ϵ where

$$\begin{bmatrix} B_a \\ A_a \\ \Gamma_a \end{bmatrix} = \begin{bmatrix} S'^2 & 2SS' & S^2 \\ C'S' & C'S + CS' & CS \\ C'^2 & 2CC' & C^2 \end{bmatrix} \begin{bmatrix} B \\ A \\ \Gamma \end{bmatrix} \tag{5.3}$$

The matrix elements C, C', S and S' are determined from two trajectory calculations for each initial phase. Figures 5.4–5.8 show the acceptance ellipses for both x and y directions for a filter with fringing fields of 0.5, 1, 2, 4 and 6 rf cycles for the operating point $a = 0.23342$ and $q = 0.706$. Ten different initial phases are illustrated in each case. The operating point is on a scan line giving a resolution of about 55. For the y direction, the alignment of the ellipses for different phases is remarkable for fringing fields greater than one rf cycle. These calculations are much more complete than the earlier ones, since the allowable transverse velocities are taken into account. Furthermore, for optimum sensitivity, the emittance of an ion source/lens system should be matched to the acceptance of the mass filter. Therefore, for both x and y directions, a converging beam is preferable (positive u associated with a negative u'). Particularly of interest are the areas in phase-space corresponding to 100% or to 50% transmission. These can be approximated by ellipses and the parameters A, B, Γ and ϵ determined (see Fig. 4.5). Appendix B lists some values for 50% transmission. These values can be used in the design of appropriate ion sources or in the evaluation of the mass filter as a detector in ion scattering experiments [10] such as secondary ion mass spectrometry (SIMS) (see Chapter X).

Assuming exact matching of the ion source to the mass filter under all conditions, the optimum relative sensitivities for fringing fields of varying lengths

References p. 119

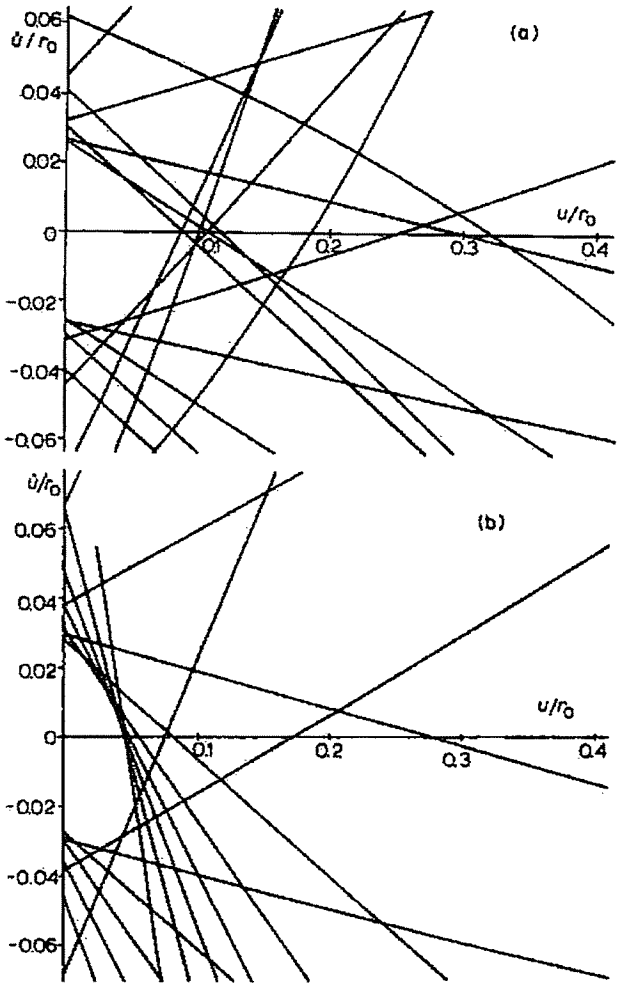

Fig. 5.4. The acceptance ellipses for the mass filter at the operating point $a = 0.2334$ $q = 0.706$ when there is a fringing field of 0.5 rf cycle. Ellipses are shown for 10 different initial phase. (a) The y direction; (b) the x direction.

can be compared by calculating the product of the acceptance areas for 50% or 100% transmission in the x and y planes. There is not a smooth variation of sensitivity with fringing field length but the general variation is shown in Fig. 5.9. A mass scale has been added for the case where all ions have the same axial energy given by $E_z = 15.5 r_0^2$ where r_0 is in centimetres and the rf frequency has been assumed to be 2 MHz. The sensitivity variation is very similar to that found experimentally [11]. The use of acceptance area for 100% transmission as a criterion for sensitivity leads to a decrease of sensitivity in proportion to the square of the resolution.

Deceleration of ions in the fringing fields by operation of the mass filter axis off ground is sometimes used to introduce slow ions which have not spent too long in the fringing fields [8].

The validity of the approximations used in obtaining Figs. 5.4–5.9 has been

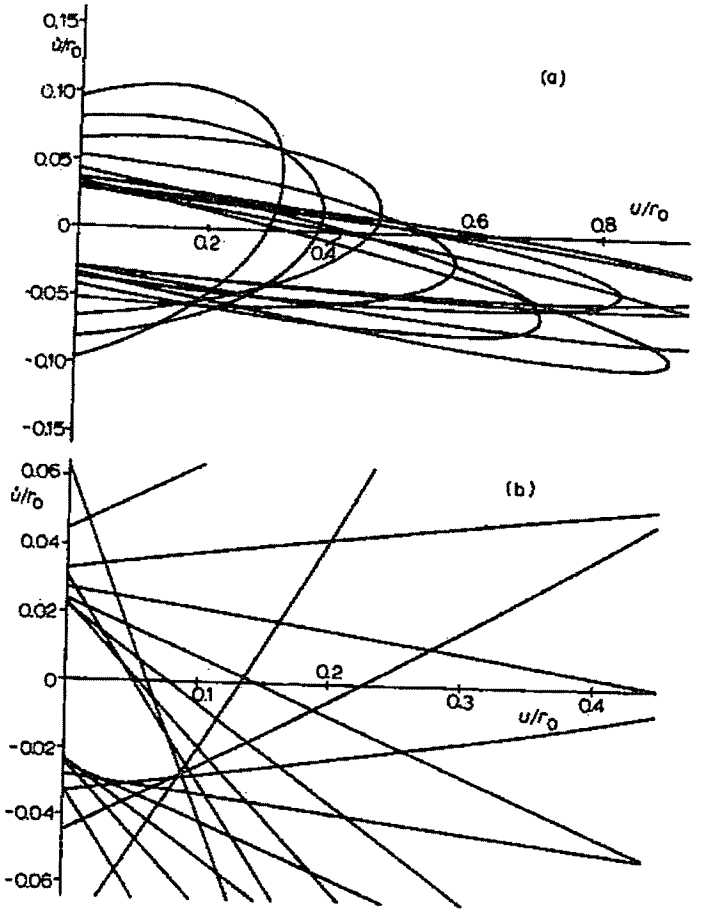

Fig. 5.5. The acceptance ellipses for ten different initial phases at the operating point $a = 0.2334$ $q = 0.706$ when the ions spend one rf cycle in the fringing field. (a) The y direction; (b) the x direction.

partially verified by spot-checks of trajectories calculated using a full three-dimensional field. The assumed potential is of the form

$$\Phi(x, y, z) = \frac{\Phi_0(x^2 - y^2)z}{r_0^3} \tag{5.4}$$

which leads to the equations of ion motion

$$\frac{d^2x}{d\xi^2} + [a - 2q \cos 2(\xi\ \xi_0)]x \frac{z}{r_0} = 0 \tag{5.5}$$

$$\frac{d^2y}{d\xi^2} - [a - 2q \cos 2(\xi - \xi_0)]y \frac{z}{r_0} = 0 \tag{5.6}$$

$$\frac{d^2z}{d\xi^2} + \frac{(x^2 - y^2)[a - 2q \cos 2(\xi - \xi_0)]}{r_0} = 0 \tag{5.7}$$

References p. 119

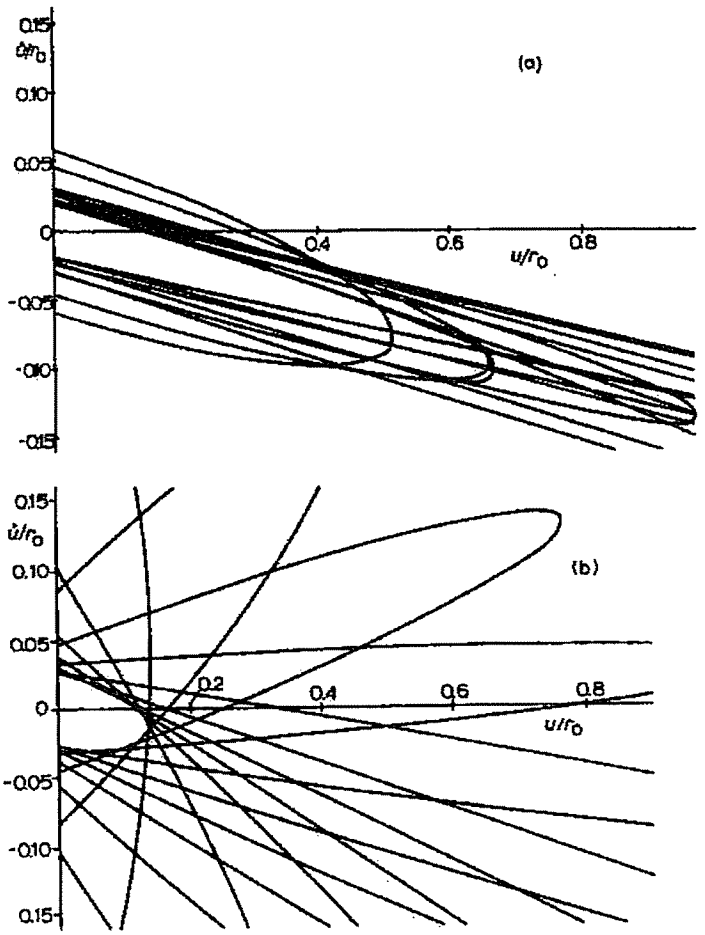

Fig. 5.6. The acceptance ellipses for (a) the y direction and (b) the x direction for the operating point $a = 0.2334$ $q = 0.706$ with a two cycle fringing field.

A similar potential would result from pole pieces rounded at the ends, but it is probably also a reasonable approximation for any case where the fringing field extends over a distance of r_0. When $(x^2 - y^2)$ is small throughout the fringing field trajectory, $dz/d\xi$ is almost constant and eqns. (5.5) and (5.6) become the usual linear approximations. When $(x^2 - y^2)$ becomes appreciable and when the initial value of $dz/d\xi$ is small, the axial velocity can be appreciably modified by the fringing field. Ions tend to be retarded, especially if their trajectory is mainly in the x quadrant, but may be accelerated if it is mainly in the y quadrant. As a result, there will be a distribution of axial velocities in the mass filter which, at high resolutions when slow-moving ions are being used, may limit the attainable resolution or contribute to peak tailing. Under some conditions, ions are reflected at the quadrupole entrance and occasionally may be trapped in the fringing fields for many rf cycles. However, these effects usually only become important for values of $u\dot{u}$ outside the 50% acceptance ellipses. The values given in Appendix B are probably quite good approximations for use in design work.

The potential given in eqn. (5.4) could be used to determine matrices of a

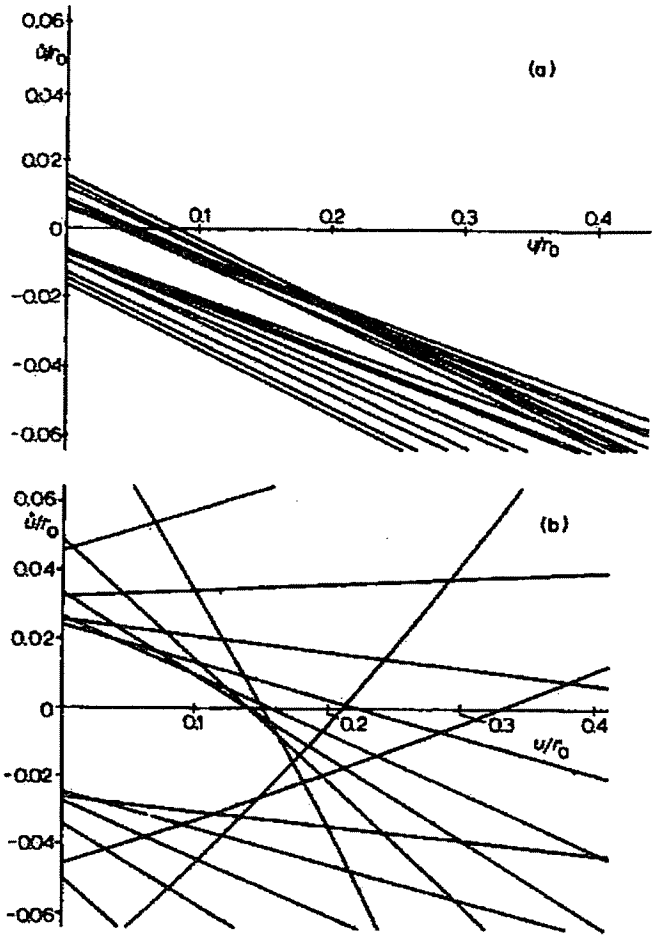

Fig. 5.7. Similar acceptance ellipses for (a) the y direction and (b) the x direction with a four cycle fringing field.

higher order than eqn. (5.2) to represent the fringing field.

An analogous situation exists at the ion exit except that now the emittance ellipses for the mass filter with exit fringing fields correspond to diverging beams (the sign of the parameter A is changed). Ions tend to be accelerated through the fringing exit fields but slow-moving ions emerging with large y values may be trapped within the fringing fields or, at certain phases, even reflected back into the device.

An example of the use of the acceptance parameters of Appendix B is illustrative of their potential value. Since allowable $\dot{u}$ values for a given u are similar even for ions with low axial velocities (Figs. 5.4–5.9), the optimum matching of the ion source requires more convergent beams for lower-velocity ions. This could be obtained with a lens, whose focal length is adjusted as the mass is scanned, between the ion source and the mass filter. A thin lens between the source, s, and the quadrupole aperture, a, gives

$$\begin{bmatrix} u_s \\ \dot{u}_s \end{bmatrix} = \begin{bmatrix} 1 & 0 \\ v_x^2/f_0 & 1 \end{bmatrix} \begin{bmatrix} u_a \\ \dot{u}_a \end{bmatrix} \tag{5.8}$$

References p. 119

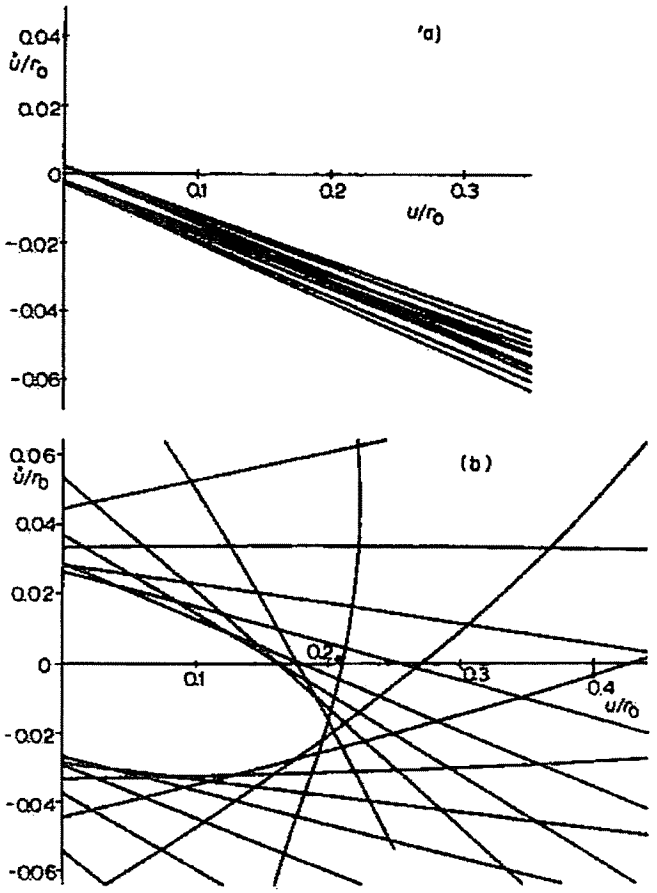

Fig. 5.8. Acceptance ellipses for (a) the y direction and (b) the x direction with a six cycle fringing field.

where f_0 is the focal length of the lens in units of r_0 and v_z is the axial velocity in units of r_0/radian of applied field. Therefore, for the 50% transmission

$$\begin{bmatrix} B_s \\ A_s \\ \Gamma_s \end{bmatrix} = \begin{bmatrix} 1 & 0 & 0 \\ -v_z/f_0 & 1 & 0 \\ v_z^2/f_0^2 & -2v_z/f_0 & 1 \end{bmatrix} \begin{bmatrix} B_a \\ A_a \\ \Gamma_a \end{bmatrix} \tag{5.9}$$

If the source is to be positioned symmetrically about the instrument axis, the axis of the source emittance ellipse should lie along the u direction. That is, $A_s = 0$ (see Chapter IV), and from eqn. (5.9)

$$\frac{1}{f_0} = \frac{A_a}{B_a}\frac{1}{v_z} \tag{5.10}$$

A_a/B_a is roughly constant for fields greater than about 1.5 rf cycles for either x or y directions. Suppose that the lens system is arranged so that v_z/f_0 is constant as was suggested above. A good value would be about 1/6 for the y direction and 1/9 for the x direction. These could be separately adjustable by use

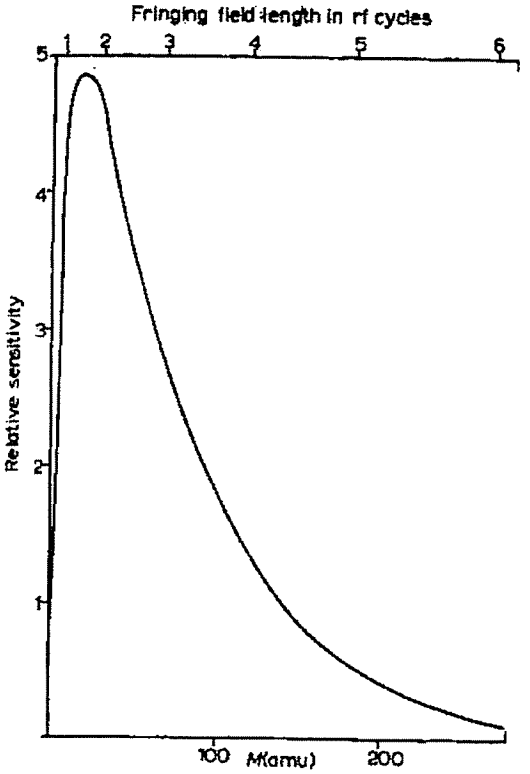

Fig. 5.9. The relative sensitivity of the mass filter as a function of the fringing field length (or of ionic mass if the axial energy is $E_z = 15.5r_0^2$) assuming good matching between the ion source emittance and the mass filter acceptance.

of an appropriate doublet or triplet quadrupole lens. Equation (5.9) can now be used to calculate the overall acceptance of the lens/fringing field/quadrupole system. Some results are shown in Fig. 5.10 which plots acceptable source combinations of u/r_0 and tan θ, the angle of divergence with the axis. This could be used to evaluate ion source designs. This very recent work has yet to be verified experimentally but seems to offer a promising and simple approach to the complex problem of overall quadrupole design.

For very slow ions, such as ions of high mass and low energy, modification of the entrance field may be necessary to obtain good sensitivities. The delayed d.c. ramp pioneered by Brubaker [1] is illustrated in Fig. 1.1(b). The original version consisted of segmented rods with short sections near the mass filter entrance to which only the rf voltages were applied. The delay in the application of the direct voltage means that as ions approach the mass filter, the (a, q) value moves first along the q axis ($a = 0$) and only later does the a value increase until the stability tip is reached when the ions enter the full quadrupole field. In this way, the ion always remains in conditions where the y trajectory is mathematically stable. Another later version, which is simpler to achieve, has four small electrodes ahead of the mass filter with appropriate d.c. voltages applied in order to partially nullify the d.c. fringing fields [3].

References p. 119

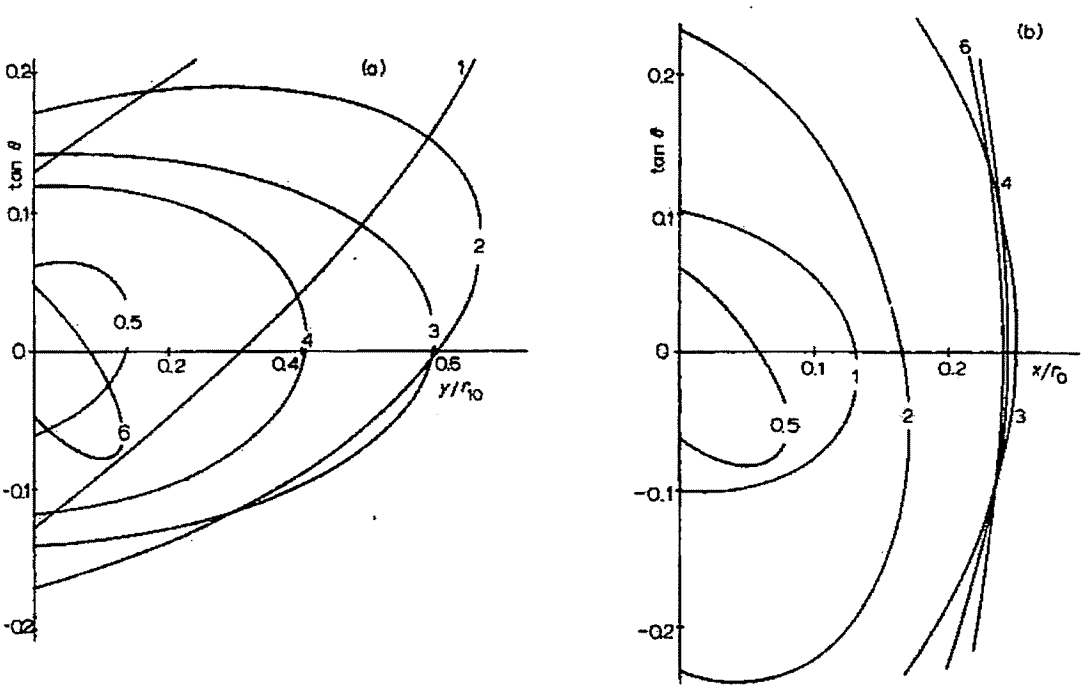

Fig. 5.10. (a) The acceptance of ions from the source given in terms of the angular divergence θ and the initial displacement y/r_0 when the lens between the source and the mass filter is always adjusted so that its focal length is given by $f_0^y = 6v_z$. The curves represent ions of different velocities (or different masses if E_z is fixed, see Fig. 5.9) and each is labelled with the length of the fringing field in rf cycles. (b) Similar acceptance curves for the x direction when the lens focal length is $f_0^x = 9v_z$.

This arrangement has the distinct advantage that the voltages applied can be adjusted empirically to "tailor" the fringing fields for optimum performance.

Figure 5.11 shows calculations of the maximum y displacements for 4.5 cycle entrance ramps with the d.c. being delayed and shortened by the number of cycles shown on each curve. There is a remarkable improvement over the coincident ramps (Fig. 5.1). The improvement in the x direction is also retained as was shown in Fig. 5.2. The ability of the mass filter to accept ions of a large range of energies has been one of its attractive features, but there is always a possibility of discrimination against slow ions if a delayed d.c. ramp is not used. No phase-space analysis of the delayed d.c. ramp mode of operation has so far been made.

The experimental evidence to support the conclusions described above is somewhat fragmentary. The only detailed measurements are those of Holme and Thatcher [12]. By combining time-of-flight, ion counting and signal averaging techniques, they were able to measure the rf modulation of the transmitted ion beam as a function of both the length of the fringing field and the resolution setting of the quadrupole. The fringing field length was varied both by changing the ion energy and by changing the separation of the ion source from the analyser. The experiments were carried out with 15 cm and 5 cm long

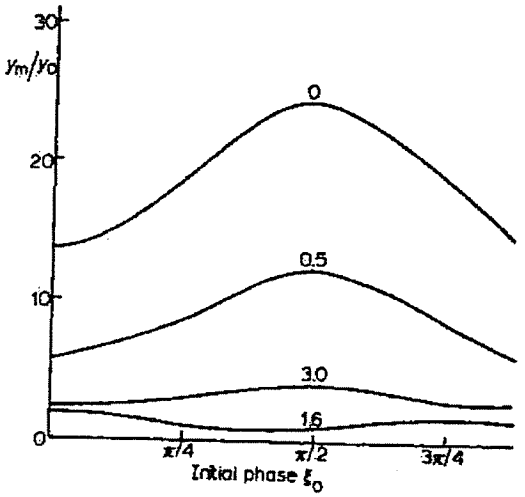

Fig. 5.11. Maximum y displacements as a function of the initial phase for the operating point $a = 0.228$ $q = 0.7$ when a delayed d.c. ramp is used. The fringing fields were 4.5 cycles long but the d.c. component was delayed by the number of cycles indicated on each curve.

analysers with $r_0 = 0.276$ cm. An example of the observed signal modulation for a short fringing field is shown in Fig. 5.12. It was found that the percentage modulation increases sharply as the number of rf cycles spent in the field approached zero. For fringing fields of more than about three rf cycles, the signal modulation was quite small. For a given fringing field length, the modulation increased as the resolution was increased. Holme and Thatcher concluded that, under normal operating conditions of most quadrupole mass filters, the phase dependence is of limited importance except perhaps at high resolution. The importance of the modulation under "normal" conditions has been disputed. Lefaivre [13], who was interested in the advantages of pulsed ion entry at the optimum phase (see Chapter II, p. 33), demonstrated that, for his mass filter, there was a high signal modulation even at low resolutions. Part of the discrepancy is probably accounted for by the difference in quadrupole size. Lefaivre's rods were hyperbolic and 110 cm long with a r_0 of 2 cm.

The other experimental evidence for the mass filter is indirect, i.e. the success of the delayed d.c. ramp. An illustration of its effectiveness, taken from the work of Brubaker [1], is given in Fig. 5.13. The 15 eV ions probably spent less than three cycles in the fringing field, but there is still an improvement at low resolutions. However, the *general* utility of the delayed d.c. ramp is still being debated (see Chapter VI, p. 144).

(2) *The monopole*

Application of the results shown in Figs. 5.1 and 5.2 to the monopole, suggests a dramatic change in instrument performance when there are fringing fields. Normally, only 50% of the ions can be transmitted because, during

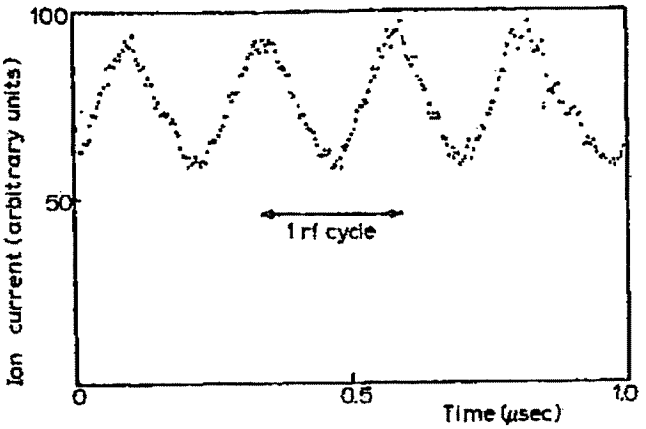

Fig. 5.12. Experimental modulation of the output signal of the mass filter when the fringing field was very short [12].

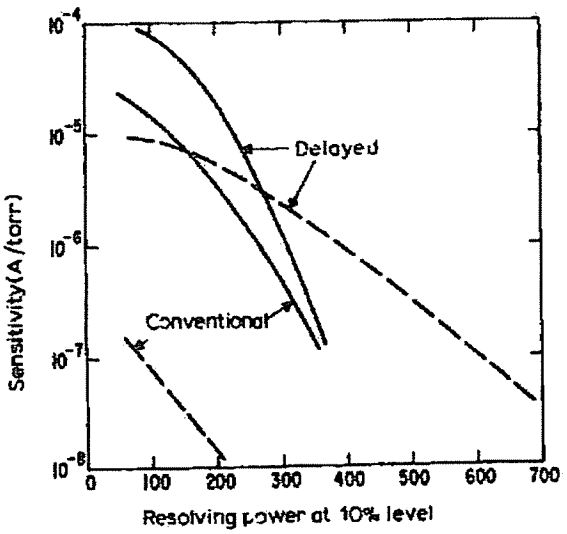

Fig. 5.13. Experimental measurements demonstrating the application of the delayed d.c. ramp technique [1]. The full curves were for 15 eV ions, the broken curves for 4 eV ions. The mass filter radius was 0.75 cm.

half the rf cycle, the ions are pushed towards the V block. Furthermore, the calculated peak shapes are very asymmetric with long "tails" on the low mass side (see Fig. 2.28). The fringing field will, by reducing the x direction ion displacement, facilitate meeting the condition $|x| < y$ and increase instrument aperture. However, more important is the change in the phase dependence of ion transmission. Figure 5.14 illustrates trajectories giving 100% ion transmission [6] for the conditions $a = 0.0825$, $q = 0.4125$ when the ions take 3.5 rf cycles to pass through a linear fringing field and 15.75 cycles to pass through the full analyser field. For clarity, only 4 phases are shown during the first part of the field, but 8 later. Trajectories are quite similar no matter what the initial field phase.

Summing the phases transmitted as one moves along a given q/a scan line gives a peak shape. Of course, this only indicates the influence on peak shape

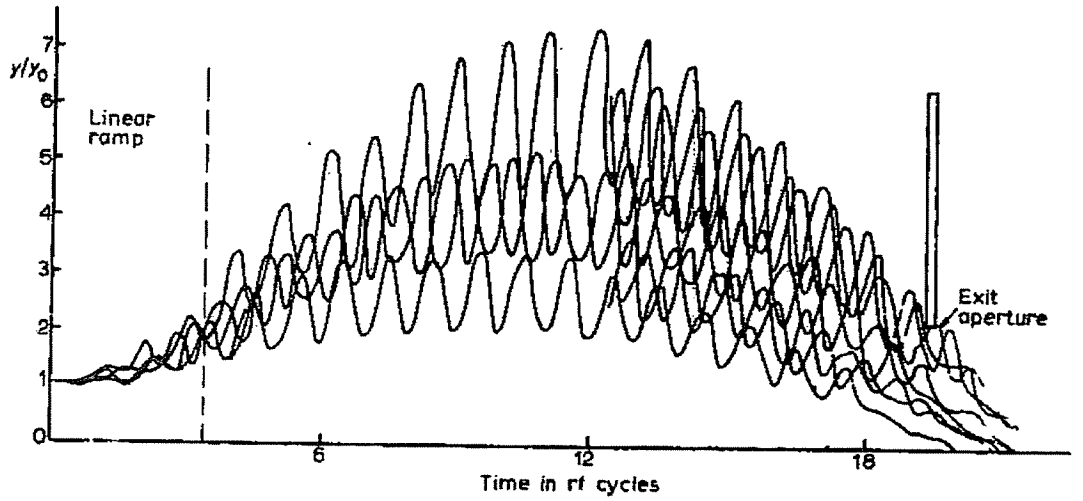

Fig. 5.14. Trajectories in the *yz* plane in the monopole for the operating point $a = 0.0825$ $q = 0.4125$ when there is a 3.5 cycle fringing field and the full analyzer field is 15.75 cycles long. Ion transmission can be 100%. Several different initial phases spread throughout the rf cycle are shown.

of the initial phase and ignores other factors such as the distribution of initial ion positions. Two results for 3.5 cycle fringes and different field lengths were given in Fig. 2.28(c). It seems likely that these calculations are closer to representing normal monopole performance than those of Fig. 2.28(a) and (b). The calculations show that a fringing field of more than 1.5 rf cycles is necessary for good performance.

A more complete view of monopole operation can be obtained by applying a phase-space analysis [13a].

There is some experimental evidence concerning fringing fields in the monopole, but it is qualitative and incomplete [6]. The output signal of a monopole was observed on an oscilloscope as the axial energy was varied. There was a distinct modulation of the signal at the rf frequency for ion energies corresponding to fringing fields less than about 1.6 rf cycles but no modulation was evident with a 2 cycle fringing field, suggesting that transmission was occurring throughout the rf cycle.

There are many problems in making phase dependence measurements but they could clearly be of considerable diagnostic value in both mass filter and monopole design. In particular, the ease of doing calculations using matrix methods (Chapter IV) provides the possibility of combining detailed performance calculations with quantitative measurements of ion transmission characteristics to arrive at an optimum instrument design.

B. SYSTEMATIC FIELD FAULTS

The question of the influence of field faults on the stability of ion trajectories was examined by von Busch and Paul [14] in the early days of

References p. 119

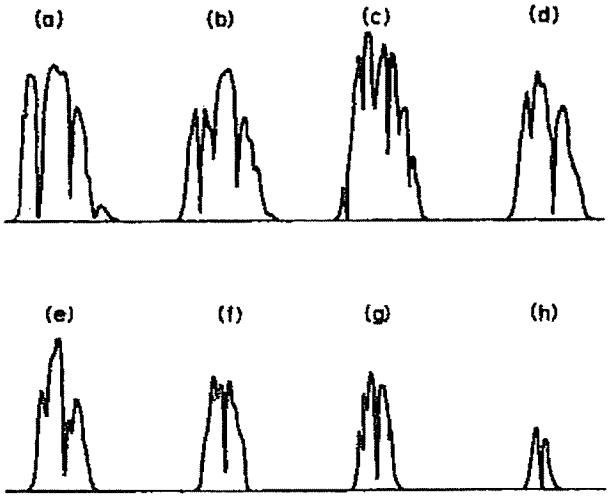

Fig. 5.15. Experimentally observed peaks in a quadrupole ion trap when the ions stayed up to 10^5 cycles in the field. The q/a value of the operating line was decreased from (a) to (h). The half-height resolution for the latter was about 18. The resonance dips can be plotted on the $a-q$ stability diagram.

quadrupole development, but the work was not widely known despite many problems with irregular peak shapes. The field faults can cause a gradual accumulation of "errors" in the ion trajectories for specific (a, q) values, so that a trajectory that would normally be stable becomes unstable or of very large amplitude. The (a, q) values where this occurs will show up in the scan of a peak (in the case of the mass filter or ion trap) as dips or shoulders. The problems will be more severe the greater the number of cycles an ion spends in the rf field and can be very severe in the ion trap operated in the selective storage mode (see Chapter II). Figure 5.15 shows a deliberately exaggerated case [15] for several scan lines of differing resolutions where ions were trapped for about 10^5 field cycles.

Von Busch and Paul showed that the "resonance dips" might be expected to occur along certain "resonance lines" in the a, q stability diagram, the position of the line depending on the type of field fault (see Fig. 5.16). The nature of these resonance lines is discussed next, using the mass filter as an example and later considering the ion trap. The extensive computer simulations are described and the experimental evidence is examined. The monopole is considered later as a special case.

(1) *The analytical approach*

In the most general case, where all types of field faults are present, the potential in the mass filter is given not by eqn. (2.9), but by a more general expression

$$\Phi = \sum_N A_N (r/r_0)^N \cos N(\phi - \phi_N)\left[U - \sum_n b_n V \cos (n\omega/2)(t - t_n)\right] \quad (5.11)$$

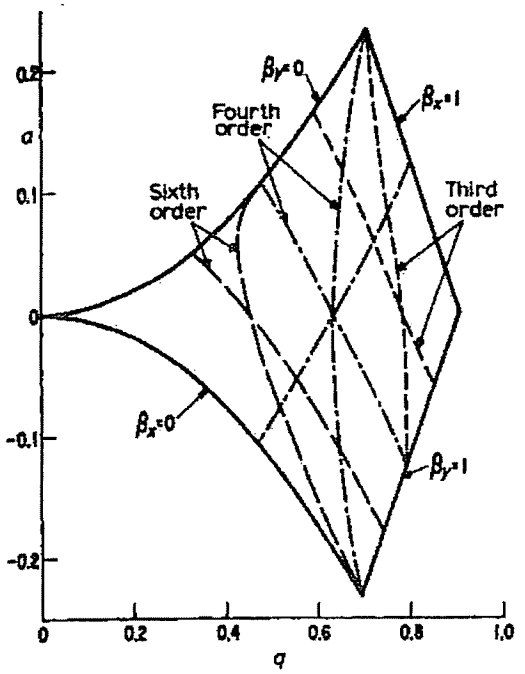

Fig. 5.16. Stability diagram for the mass filter showing the resonance lines caused by third, fourth- and sixth-order field distortions. Only one of the two possible third-order distortions is shown.

where r and ϕ are polar co-ordinates, A_N and b_n are weighting factors and the t_n are phase factors. For the ideal field, the only terms are those with $N = n = 2$ and eqn. (5.1) transforms into eqn. (2.9). Terms that have both $N \neq 2$ and $n \neq 2$ can be neglected. Consider first the case $n = 2$, that is, the time-varying term is purely sinusoidal and the field faults are geometric. In addition to the usual second-order term with $N = 2$, for which we take $A_2 = b_2 = 1$, there are higher-order terms. An N of three gives a term representing a hexapole field. Converting to Cartesian co-ordinates

$$\Phi_3 = \frac{A_3}{r_0^3}(3yx^2 - y^3)[U - V\cos\omega(t - t_2)] \tag{5.12}$$

Note that Laplace's equation is still obeyed but the restoring force on an ion is no longer linearly dependent on its displacement from the centre. There is also a coupling of motion in the x and y directions. The third order term is asymmetric with respect to the x and y directions. There are two possible third-order distortions. Figure 5.17(a) shows how the equipotential lines would be modified by the presence of a large third-order distortion with $A_3 = 3r_0$. A contribution of the third-order type would evidently be produced by an asymmetric positioning of one of the electrodes.

A fourth-order, or octopole, term with $N = 4$, is given by

$$\Phi_4 = \frac{A_4}{r_0^4}(x^4 - 6x^2y^2 + y^4)[U - V\cos\omega(t - t_2)] \tag{5.13}$$

References p. 119

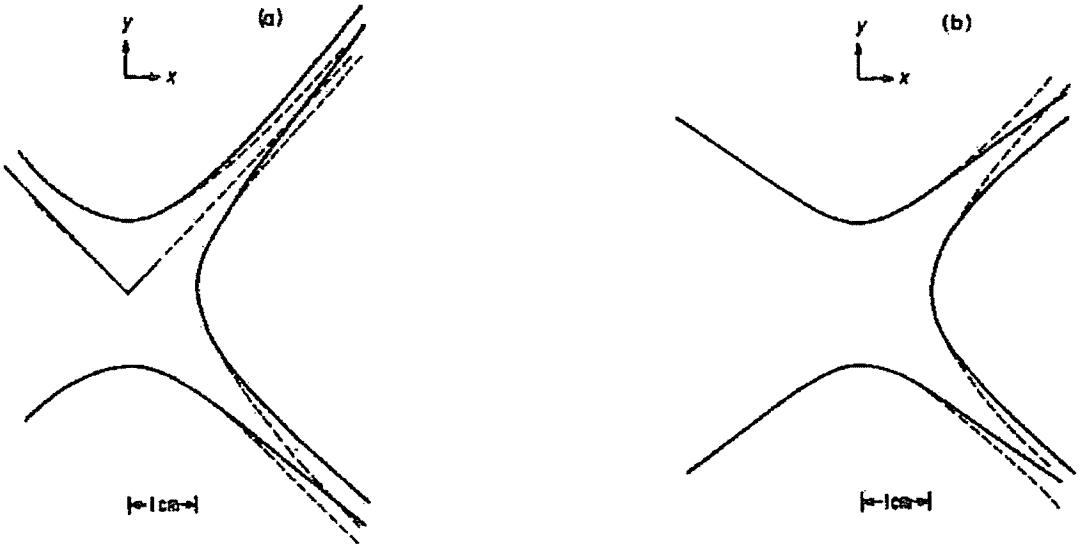

Fig. 5.17. (a) The solid lines are equipotential contours for the mass filter in the presence of a third-order distortion with a weighting factor $A_3/r_0 = 3$. The broken lines are equivalent contours with no field distortion. (b) Equipotential contours when there is a fourth-order distortion with a weighting factor $A_4/r_0^3 = 100$.

and Fig. 5.17(b) illustrates the kind of geometric error that is involved.

Higher-order terms are generally less significant but one of potential importance is the sixth-order distortion. This is the principal fault caused by the common use of round instead of hyperbolic rods. The sixth-order term is

$$\Phi_6 = \frac{A_6}{r_0^6}(x^6 - 15x^4y^2 + 15x^2y^4 - y^6)[U - V\cos\omega(t - t_2)] \qquad (5.14)$$

Figure 5.18 shows how the round rod structure can be well represented by the addition of an appropriate sixth-order term.

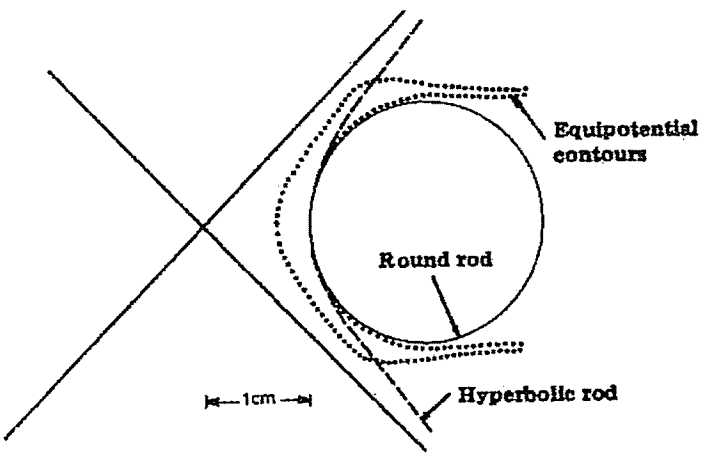

Fig. 5.18. Equipotential contours showing how the use of a round rod instead of a hyperbolic rod can be well represented by including a sixth-order term with a weighting factor $A_6/r_0^4 = 10^6$.

In the ion trap, the third- and fourth-order terms are similarly given [15] by

$$\Phi_3 = \frac{A_3}{4z_0^3}(3r^2z - 2z^3)[U - V\cos\omega(t - t_2)] \tag{5.15}$$

$$\Phi_4 = \frac{A_4}{4z_0^4}(r^4 + \tfrac{8}{3}z^4 - 8r^2z^2)[U - V\cos\omega(t - t_2)] \tag{5.16}$$

From the general theory of harmonic oscillators [14], one can deduce that the higher-order geometric terms produce sum resonances at those conditions where (for the mass filter)

$$\frac{\beta_x}{2}K + (N-K)\frac{\beta_y}{2} = 1 \tag{5.17}$$

where K can have the values $N, N-2, N-4, \ldots$ Thus the third-order resonance lines occur at

$$\beta_x = \frac{2}{3} \quad \text{and} \quad \frac{\beta_x}{2} + \beta_y = 1 \tag{5.18}$$

and evidently since the distortion is asymmetric, there is the other possibility

$$\beta_y = \frac{2}{3}, \quad \frac{\beta_y}{2} + \beta_x = 1 \tag{5.19}$$

The fourth-order resonances are at

$$\beta_x = \tfrac{1}{2}, \quad \beta_x + \beta_y = 1 \quad \text{and} \quad \beta_y = \tfrac{1}{2} \tag{5.20}$$

and the sixth-order distortion produces resonances at

$$\beta_x = \tfrac{1}{3}, \quad \beta_y = \tfrac{1}{3}, \quad 2\beta_x + \beta_y = 1, \quad \beta_x + 2\beta_y = 1 \tag{5.21}$$

Some of the resonance lines were shown in Fig. 5.16 for the mass filter and some corresponding lines for the ion trap are given in Fig. 5.19. The lines that pass through the tip of the stability diagram are particularly important.

The analytic theory gives the location of the resonance lines but does not indicate how severe the effects might be for a given amount of distortion. This can, however, be estimated by computer simulation.

The terms in eqn. (5.11) with $N = 2, n > 2$ representing harmonics in the rf supply are generally not very important. If the additional terms are sufficiently large, there will be a modification in the position of the zone of stability (see Chapter III). However, odd harmonics of the sub-frequency $\omega/2$, which may be present in circuits which use frequency doubling [14], might cause resonance lines at $\beta = 1/2$.

(2) *Computer simulation*

The technique of computer simulation of ion trajectories by numerical integration of the equations of motion (Chapter IV) has been applied to dis-

References p. 119

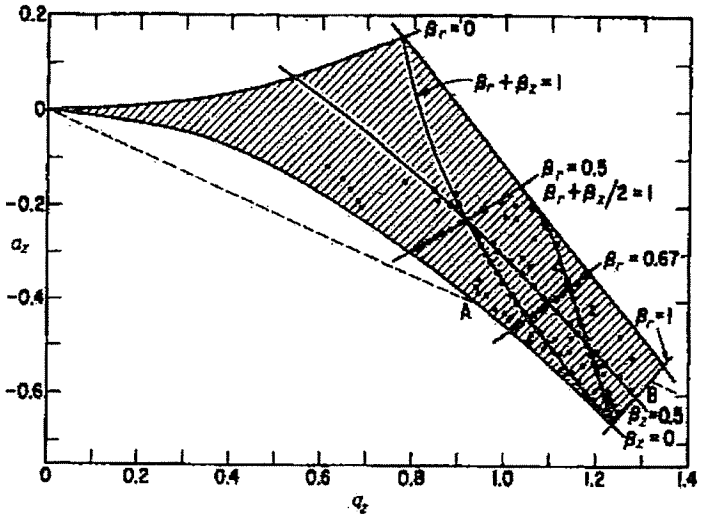

Fig. 5.19. Stability diagram for the ion trap showing the resonance lines caused by third- and fourth-order distortion. The points represent experimental measurements. The principal resonance dips fall on the theoretically predicted curves.

torted fields. The calculations are more complex since x and y motions are no longer independent. They have been carried out in detail only for one particular initial phase of the rf field. Figure 5.20 shows the peak shapes that are theoretically obtained with various scan lines for the ion trap operated in the selective trapping mode (see Chapter II), assuming that a maximum displacement of ten times the initial value is permissible before an ion is lost from the trap. Ions were considered to be accumulated during $200/\pi$ rf cycles and there was a third-order field distortion with a weighting factor A_3 equal to $10z_0/3$. The peak splitting becomes more severe as one approaches the tip of the stability diagram. If the positions of the principal resonance dips are plotted on an $a-q$ diagram, one can see a general agreement with the analytical theory. The field distortions also appear to produce a "blunting" of the tip of the stability diagram which would limit the attainable resolution. Such a limit is experimentally observed with ion traps of approximate geometry. Similar calculations have been made for both third- and fourth-order distortions in the mass filter [16].

The degree of field imperfection that can be tolerated in obtaining a given performance can be estimated from these calculations recalling, however, the limitation that only one initial phase has so far been considered. The results are presented in Fig. 5.21(a)–(c), as the number of rf cycles before an ion at the (a, q) position of the main resonance dip will exceed ten times its initial displacement versus the appropriate distortion weighting factor. The requirements are more severe the higher the resolution. Figure 5.21(a) is for a third-order distortion in the ion trap. At low pressures, the accumulation time in the ion trap is often very long (see Chapter VIII) even at low resolution and geometric distortions are very important. Figure 5.21(b) and (c) are for dis-

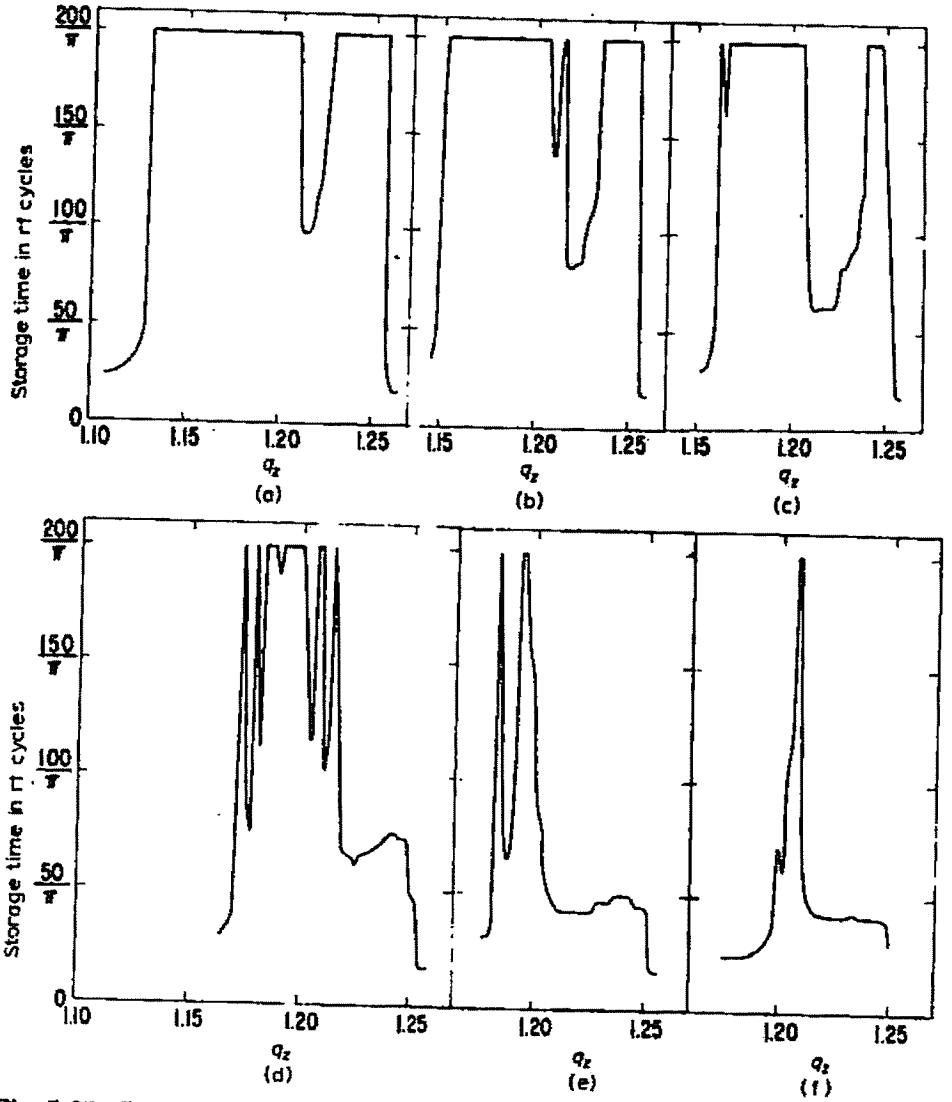

Fig. 5.20. Computed peak shapes for various operating lines in the ion trap in the presence of a third-order distortion with a weighting factor $A_3 = 10z_0/3$. The operating lines had the following q/a ratios: (a) 2.025; (b) 2.0; (c) 1.9875; (d) 1.975; (e) 1.9625; and (f) 1.95.

tortions in the mass filter. The broken lines represent von Zahn and co-workers' [17] criterion for an optimum quadrupole performance; that is, the resolution R is limited to $n^2/12.25$ where n is the number of cycles within the field. Using this criterion, which is more favourable than that often found (see Chapter VI, p. 123), the intersection of the lines indicates the degree of distortion that can be tolerated. The results are summarized in Fig. 5.22. For low performance, gross distortions are permissible, but conditions become stringent at high resolution [18] due to the combination of closer approach to the limit of the stability diagram and the necessity for more rf cycles in the field. Experimental evidence is presented in Chapter VI, Fig. 6.3, which is in accord with the theory.

References p. 119

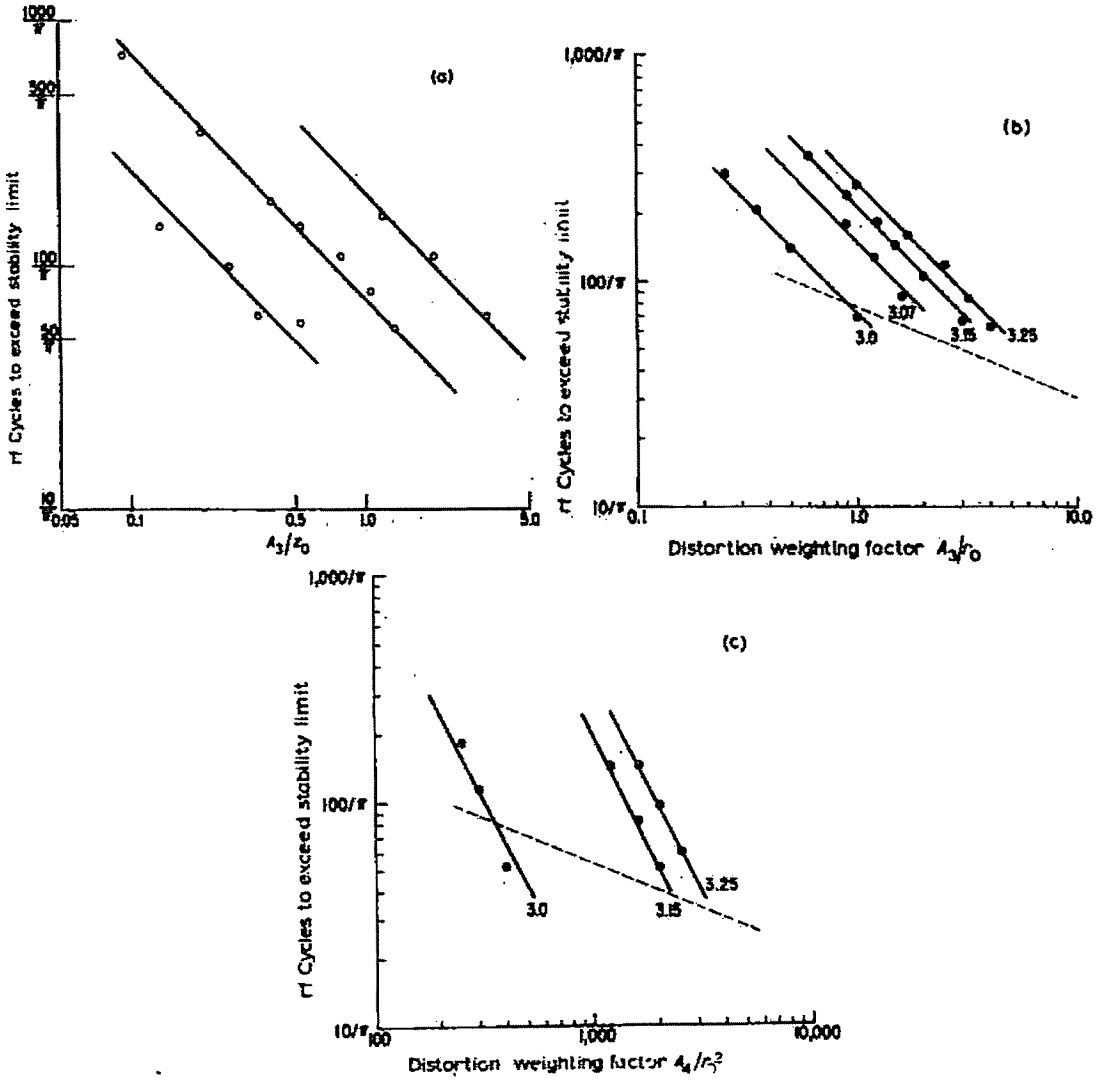

Fig. 5.21. (a) A log–log plot of the number of rf cycles needed before the stability limit is exceeded in the ion trap at the a, q position of the third-order resonance dip versus the distortion weighting factor. The curves are for operating lines having nominal resolutions of 10, 26 and 52. (b) Similar curves for a mass filter with third-order distortions. The q/a ratios are given on each curve and correspond to nominal resolutions of 54, 20, 12 and 8. The broken line gives von Zahn's criterion for maximum quadrupole performance, i.e. $R = n^2/12.25$. (c) A similar plot for a fourth-order distortion in the mass filter.

(3) *Experimental evidence*

Some good "bad" examples of split peaks for the ion trap have already been shown in Fig. 5.15. If the positions of dips are plotted on a stability diagram for many different scan lines, Fig. 5.19 is obtained and the most pronounced resonance dips fall on the expected resonance lines [19]. The origin of the resonance lines as third- and fourth-order distortions has been confirmed by changing the spacing of the end-cap electrodes in an asymmetric or

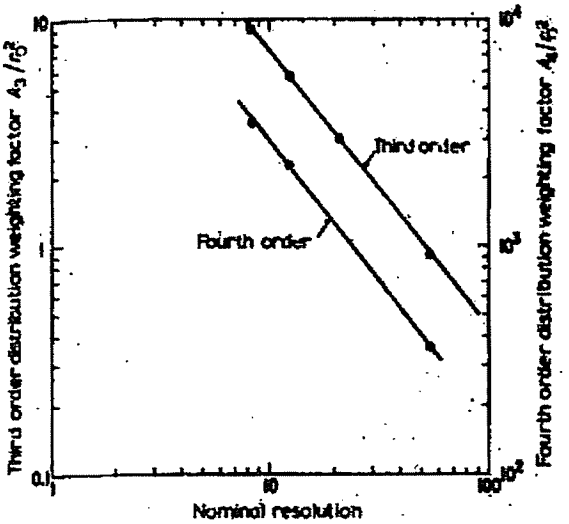

Fig. 5.22. Using von Zahn's criterion for optimum quadrupole performance, the maximum tolerable field distortions are plotted as a function of the resolution. Note the different ordinates for third- and fourth-order distortions.

symmetric way and observing the changes in the importance of the resonance dips.

Plotting the experimentally observed resonance dips on the stability diagram can be used as a diagnostic technique for determining which field faults are present.

For the ion trap, it was observed empirically [20] that a small bias applied between the end-caps (usually a few per cent of the d.c. voltage applied to the ring electrode) produced an improved peak shape. This was explained as being due to a slight shift in the stability diagram to higher q values, with little change in the positions of the resonance lines. The hypothesis has been confirmed [16] both by experimental observation and by computer simulation. Less bias is required at high resolutions since a very small shift removes the tip of the stability diagram from the position of the resonance lines. The computer simulations suggest some loss of sensitivity accompanying the use of a bias voltage. In experiments with various mesh ion traps [21] of very approximate geometry, it is found that good performance can sometimes be obtained without application of a bias between the end caps and this seems to be also associated with resonance lines that no longer pass exactly through the tip of the stability diagram. The geometric origins of such a shift are not clear.

(4) *Round rods*

In most quadrupole mass filters, round rods have been used instead of the correct hyperbolic rods. The optimum size for the rods is the radius $r = 1.148r_0$ where r_0 is the field radius [22, 23]. A value of $r = 1.16r_0$ has often been misquoted and calculations show that the larger rods may reduce the useful

aperture of the instrument. Figure 5.18 illustrates how the round rods produce a sixth-order (and smaller tenth-order) distortion. Denison [23] has suggested that the sixth-order distortion can be minimized by using round rods of appropriate radius in conjunction with a grounded cylindrical housing. For example, the distortion is near zero when $r = 1.1468r_0$ and the cylindrical housing radius $R = 3.54r_0$. Similar calculations for optimizing the r/r_0 ratio have been made for the four-fold monopole illustrated in Fig. 1.1(h) [24].

Dawson and Whetten [25] estimated from Fig. 5.22 that the sixth-order resonance lines caused by round rods might become significant at resolutions greater than a few hundred. They suggested that such resonance might lie at the origin of the pre-cursor peaks often observed at high resolution, since the resonance line $\beta_x + 2\beta_y = 1$ is close to the y stability boundary. High resolution without pre-cursor problems might result from slight and inadvertent asymmetries between opposite rods which shift the stability boundaries as described above for the ion trap. However, Leck and co-workers [26] find that the occurrence of the precursor peak is not systematic enough to be explained in this way.

The only reported experiments comparing directly the performance achieved using round and hyperbolic rods in the same mass filters are by Brubaker [27, 28]. These are difficult experiments because of the variations that sometimes occur even when a particular mass filter is dismantled and reassembled. Brubaker's results are illustrated in Fig. 6.4. The delayed d.c. ramp (see p. 105) was used in both cases. For a given sensitivity, the resolution can be augmented by a factor of two by the use of hyperbolic rods. Undoubtedly, several manufacturers have experimented with hyperbolic rods, but it seems that in instruments of moderate performance, any gains do not offset the costs of increased complexity in manufacture (see Chapter VI, p. 129 for further discussion).

(5) *Field distortions and the monopole*

Since the scan line for the monopole does not have to pass through the tip of the stability diagram (Fig. 2.24), resonance lines are not important. The q/a ratio for the scan line can be chosen to avoid all resonance lines in the neighbourhood of the y stability boundary. However, the field distortions will affect the focussing qualities of the monopole [3] and of the instruments which utilize the focussing properties of quadrupole fields (see Chapter II). In the absence of fringing fields, the monopole, as described in Chapter II, has rather poor focussing in the yz plane. At the position of optimum focussing (Fig. 2.25), the trajectories for those initial rf phases which give the maximum displacement are also farthest from the axis at the exit aperture. A slight third-order distortion ($A_3/r_0 \leqslant +0.5$) caused by a closer positioning of the rod to the V block will give a stronger than usual field for the larger ion displacements and actually improve the focussing. However, monopole operation

is so little documented in detail, and apparently so dependent on fringing fields, that these theoretical subtleties are best left in abeyance.

REFERENCES

1 W.M. Brubaker, Advan. Mass Spectrom., 4 (1968) 293.
2 W.M. Brubaker, Proc. 5th Int. Instrum. Conf., Stockholm, 1960.
3 W.M. Brubaker, J.Vac. Sci. Technol. 10 (1973) 291. (Abstract)
4 P.H. Dawson, J. Vac. Sci. Technol., 8 (1971) 263.
5 P.H. Dawson, Int. J. Mass Spectrom. Ion Phys., 6 (1971) 34.
6 P.H. Dawson, J. Vac. Sci. Technol., 9 (1972) 487.
7 P.H. Dawson, Int. J. Mass Spectrom. Ion Phys., 14 (1974) 317.
8 P.H. Dawson, Int. J. Mass Spectrom. Ion Phys., 17 (1975) 423.
9 K.G. Steffen, High Energy Beam Optics, Interscience, New York, 1965.
10 P.H. Dawson, Int. J. Mass Spectrom. Ion Phys., 17 (1975) 447.
11 T.C. Ehlert, J. Phys. E, 3 (1971) 237.
12 A.E. Holme and W.J. Thatcher, Int. J. Mass Spectrom. Ion Phys., 10 (1972/3) 271.
13 D. Lafaivre, M.Sc. Thesis, Laval University, 1973.
13a R. Baribeau and P.H. Dawson, to be published.
14 F. von Busch and W. Paul, Z. Phys., 164 (1961) 581.
15 P.H. Dawson and N.R. Whetten, Int. J. Mass Spectrom. Ion Phys., 2 (1969) 45.
16 P.H. Dawson and N.R. Whetten, Int. J. Mass Spectrom. Ion Phys., 3 (1969) 1.
17 W. Paul, H.P. Reinhard and U. von Zahn, Z. Phys., 152 (1958) 143.
18 M.S. Story, J. Vac. Sci. Technol., 4 (1967) 326. (Abstract)
19 N.R. Whetten and P.H. Dawson, J. Vac. Sci. Technol., 6 (1969) 100.
20 P.H. Dawson and N.R. Whetten, J. Vac. Sci. Technol., 5 (1968) 11.
21 P.H. Dawson and C. Lambert, unpublished results.
22 I.E. Dayton, F.C. Shoemaker and R.F. Mozley, Rev. Sci. Instrum., 25 (1954) 485.
23 D.R. Denison, J. Vac. Sci. Technol., 8 (1971) 266.
24 A.B. Birtles and D.J. Mellor. J. Phys. E., 5 (1972) 1203.
25 P.H. Dawson and N.R. Whetten, J. Vac. Sci. Technol., 7 (1970) 440.
26 A.E. Holme, W.J. Thatcher and J.H. Leck, J. Phys. E., 5 (1972) 429.
27 W.M. Brubaker, 16th Annu. Conf. Mass Spectrom. Allied Topics, Pittsburg, 1968.
28 W.M. Brubaker, J. Vac. Sci. Technol., 4 (1967) 326. (Abstract)

FILED UNDER SEAL – SUBJECT TO PROTECTIVE ORDER
CONTAINS CONFIDENTIAL MATERIAL

IN THE UNITED STATES DISTRICT COURT
FOR THE DISTRICT OF DELAWARE

APPLERA CORPORATION, MDS INC., and APPLIED BIOSYSTEMS/MDS SCIEX,	**Civil Action No. 00-CV-105**
Plaintiffs,	**HON. RODERICK McKELVIE**
v.	**MAGISTRATE THYNGE**
MICROMASS UK LTD., and MICROMASS, INC.,	
Defendants.	

DEFENDANTS' OPENING CLAIM CONSTRUCTION BRIEF

Filed: November 9, 2001

Robert W. Whetzel (#2288)
Chad Shandler (#3796)
RICHARDS, LAYTON & FINGER
One Rodney Square
P.O. Box 551
Wilmington, DE 19899
(302) 658-6541

James G. Hunter, Jr.
Kenneth G. Schuler
Kevin C. May
LATHAM & WATKINS
Sears Tower, Suite 5800
Chicago, IL 60606
(312) 876-7700

ATTORNEYS FOR DEFENDANTS
MICROMASS UK LTD. AND
MICROMASS, INC.

> in the specification an adequate disclosure showing what is meant by that language. If an applicant fails to set forth an adequate disclosure, the applicant has in effect failed to particularly point out and distinctly claim the invention as required by the second paragraph of section 112.

In re Donaldson Co., 16 F.3d 1189, 1195 (Fed. Cir. 1994). The Federal Circuit therefore has emphasized that "[i]t is the disclosures of the applicants that count" in determining whether an invention is adequately set forth in the specification for purposes of the "written description" requirement of § 112, and that which allegedly is known to those of skill in the art cannot make up for what a patentee failed to disclose. See Lockwood v. American Airlines, Inc., 107 F.3d 1565, 1571-72 (Fed Cir. 1997). Because the specification does not identify differential pumping as a structure associated with directing ions through the inlet orifice, Plaintiffs' construction of "means . . . for directing" should be rejected.

L. "End To End"/"Aligned"

Claim Element 1(c) of the '736 Patent requires that "said first rod set be[] located ***end to end*** with said second rod set so that said first and second spaces are ***aligned***." The ordinary meaning of the phrase "end to end" is, according to a leading dictionary, "characterized by having the end of one object placed against the end of another." WEBSTER'S THIRD NEW INTERNATIONAL DICTIONARY at 750. See also POCKET OXFORD DICTIONARY OF CURRENT ENGLISH at 285 ("with the end of one adjoining the end of the next in a series"). Nothing in the patent specification indicates that this phrase is to be given a meaning different from its ordinary meaning. See '736 Patent (Ex. 2) at Col. 1-14 (A79-A85). Thus, Claim Element 1(c) requires that the end of the first rod set be placed at or near the end of the second rod set.

Not only is this understanding of "end to end" consistent with its ordinary meaning, it is mandated by the second portion of the claim element which specifies that positioning the rod sets end to end results in the spaces defined by those rod sets being "aligned." Plaintiffs discussed the term "aligned" at length during reexamination in connection with the

prosecution of Claims 25 and 26, which are dependent upon Claim 1. See Aug. 12, 1998 Response After Final Office Action (Ex. 21) at 2-4 (A355-A357). Claim 25 requires that "a first longitudinal axis of the first rod set intersect[] a second longitudinal axis of the second rod set." Amendment (Ex. 14) at 2 (A269). Claim 26 requires that "the first rod set [be] parallel to the second rod set." Id. The Examiner initially rejected Claims 25 and 26 for indefiniteness and for failing to add any further limitation to the claimed invention. See June 15, 1998 Office Action in Reexamination (Ex. 16) at 2 (A326). The Examiner found Claim 25 indefinite because, as he put it, "[h]ow can the two longitudinal axes or the rod sets intersect if they are aligned?" Id. He rejected Claim 26 because "if the two rod sets are aligned, they are by definition parallel." Id.

To overcome the Examiner's rejection, Plaintiffs argued that "[t]he use of the term 'aligned' in Claim 1 . . . does not necessarily mean that the first and second rod sets are *parallel* to each other" because "[t]he first and second spaces, for instance, may be ***'aligned' when an end of the first space terminates near an end of the second space.***" Aug. 12, 1998 Response After Final Office Action (Ex. 21) at 2-3 (A355-A356). Thus, according to Plaintiffs, "the first space could be at an angle relative to the second space and the two spaces could be ***aligned by having the ends precisely located relative to each other so that their ends abut***." Id. at 4 (A357) (underline emphasis added). Plaintiffs, accordingly, made two separate points about what is meant by the first and second spaces being "aligned": First, they made it clear that it does not mean that the spaces must share a common axis. Second, they indicated that the spaces are "aligned" for purposes of the patent when their ends abut one another. After Plaintiffs made these arguments, the Examiner allowed Claims 25 and 26. See Reexamination Certificate (Ex. 18) (A330-A331).

Plaintiffs are bound by their previous construction of "aligned" for purposes of this litigation. See Southwall Technologies, 54 F.3d at 1576 ("Claims may not be construed one

way in order to obtain their allowance and in a different way against accused infringers."). Thus, given that the spaces defined by the rod sets must be abutting, "end to end" must mean that the end of the first rod set is placed at or near the end of the second rod set. Not only is this construction consistent with the plain meaning of "end to end," it is the only construction that conforms with the meaning of "aligned."

Remarkably, Plaintiffs now construe "end to end" as meaning that "the two rod sets are positioned in such a fashion so as to ***axially align*** the elongated spaces defined by the two rod sets." Pl. Supp. Resp. to Interrog. No. 2 (Ex. 19) at 9 (A340). Plaintiffs' proposed construction necessarily should be rejected given that it squarely contradicts the construction Plaintiffs relied on during the reexamination proceedings. It bears emphasizing that Claims 25 and 26 are dependent upon – and therefore contain all the limitations of – independent Claim 1. In order to obtain allowance, Plaintiffs had to ***harmonize*** the language of Claim 1 – which requires that "said first rod set be[] located end to end with said second rod set so that said first and second spaces are aligned" – with the language of those dependent claims (which require that the axes of the rod sets intersect or that the rod sets be parallel to one another). See disc. supra at 38.

Plaintiffs offered but one possible harmonizing construction of the claim language at issue. Based upon what they described as the "common, accepted meaning of 'aligned,'" (Aug. 12, 1998 Response After Final Office Action (Ex. 21) at 3 (A356)), Plaintiffs rejected the Examiner's suggestion that Claim 1 implied that the spaces be in ***axial*** alignment, and argued that "aligned" instead means that the ends of the first and second spaces must abut. See disc. supra at 38. In fact, they expressly stated that "the first space could be at an angle relative to the second space." Ex. 21 at 4 (A357). Thus, not only does Plaintiffs' proposed construction of

"end to end" ignore the plain meaning of that phrase, it is impermissible because it conflicts with their binding statements during reexamination.

Similar to Claim 1, Claim 14 requires "first and second spaces . . . located ***end-to-end*** with each other and separated by an interchamber orifice so that an ion may travel through said first space, said interchamber orifice and second space . . . ." Claim Element 14(preamble). Thus, pursuant to the plain meaning of "end to end," the end of the first space must be located at or near the end of the second space. This construction is confirmed by other portions of the claim which emphasize the relative proximity of the two spaces by indicating that they are separated only by an interchamber orifice. See, e.g., Claim Element 14(preamble) (A86). For example, the claim recites that ions travel "***first*** through said first space, said interchamber orifice ***and then*** through said second space. . . ." Claim Element 14(b). By specifying the specific sequence in which the ions will encounter these elements, the patent makes clear that the end of the first space is located at or near the end of the second space.

M. Claim Elements 1(d) and 14(b)

Claim Elements 1(d) and 14(b) are quite similar. Claim Element 1(d) recites "an interchamber orifice located in said wall and aligned with said first and second spaces so that ions may travel through said inlet orifice, through said first space, through said interchamber orifice, and through said second space." The preamble to Claim 14 specifies that the first and second vacuum chambers are "separated by an interchamber orifice," and Claim Element 14(b) requires a method of "directing said ions through an inlet orifice in an inlet wall into said first space, first through said first space, said interchamber orifice and then through said second space, and then detecting the ions which have passed through said second space." We examine the foregoing claim language below.

CONCLUSION

For the foregoing reasons, Micromass respectfully submits that the terms in the patent claims at issue should be construed as indicated herein.

Date: November 9, 2001

By _____ (#3796)
One of the Attorneys for Micromass UK Ltd. and Micromass Inc.

Robert W. Whetzel
Chad Shandler
RICHARDS, LAYTON & FINGER
One Rodney Square
P.O. Box 551
Wilmington, DE 19899

James G. Hunter, Jr.
Kenneth G. Schuler
Kevin C. May
LATHAM & WATKINS
Sears Tower, Suite 5800
Chicago, IL 60606
(312) 876-7700